



**Remarkably Improved Electrochemical Hydrogen Storage of
Multi-walled Carbon Nanotubes Decorated with Nanoporous
Bimetallic Fe-Ag/TiO₂ Nanoparticles**

Journal:	<i>Dalton Transactions</i>
Manuscript ID	DT-ART-09-2018-003897.R1
Article Type:	Paper
Date Submitted by the Author:	24-Oct-2018
Complete List of Authors:	akbarzadeh, raziye; university of kashan, chemistry; Ghaedi, Mehroang; university, Nasiri Kokhdan, Syamak; University of Kashan, Chemistry Vashae, Daryoosh; North Carolina State University, ECEN



Journal Name

ARTICLE

Remarkably Improved Electrochemical Hydrogen Storage of Multi-walled Carbon Nanotubes Decorated with Nanoporous Bimetallic Fe-Ag/TiO₂ Nanoparticles

Received 00th January 20xx,
Accepted 00th January 20xx

DOI: 10.1039/x0xx00000x

www.rsc.org/

Raziyeh Akbarzadeh,^a Mehrorang Ghaedi, *^a Syamak Nasiri Kokhdan,^a Daryoosh Vashae^b

Nanoporous bimetallic Fe-Ag nanoparticles (NPs) were synthesized using a facile chemical reduction method and used to decorate the surface of multi-walled carbon nanotubes (MWCNTs) for hydrogen sorption and storage. The effect of TiO₂ nanoparticles on the Fe-Ag/CNTs hydrogen storage properties were further studied in details. For this purpose, several nanocomposites of nanoporous bimetallic Fe-Ag/TiO₂ nanoparticles with different amounts of bimetallic Fe-Ag NPs were prepared via hydrothermal method. The hydrogen storage capacity of the as-prepared nanocomposites were studied using electrochemical methods. The Fe-Ag/TiO₂/CNT nanocomposite with the 0.04 M of bimetallic Fe-Ag NPs showed the highest capacity for hydrogen storage which was ~5X higher than the pristine MWCNTs. The maximum discharge capacity was 2931 mAh g⁻¹ corresponding to 10.94 wt% hydrogen storage capacity. Furthermore, a 379% increase in discharge capacity was measured after 20 cycles. These results show that Fe-Ag/TiO₂/CNT electrode displays superior cycle stability and high reversible capacity, which is attractive for battery applications.

1. Introduction

Hydrogen energy is researched extensively as an alternative to fossil fuels because of critical advantages such as large combustion heat 287 kJ/mole, abundant supply, renewability, high efficiency, environmentally compatible by-product, water, and greenhouse gases emission, etc.^{1,2} However, design and development of appropriate hydrogen storage materials with long-lasting stability toward future of energy is a most scientific challenge which dominates in the foundation of hydrogen economy.³⁻⁵ Sodium borohydride (NaBH₄) emerged as a new and promising hydrogen storage material.⁶⁻⁸

In recent years, great attention was devoted to the development of new porous materials with high ability of hydrogen sorption such as Carbon nanotubes (CNTs), graphene and few-layer graphene.⁹⁻¹² CNTs are a good choice for electrochemical hydrogen storage due to their unique physical and chemical properties, such as high specific surface area, impressive chemical stability, high mechanical ability, low density and high electron-transfer rate.^{13,14}

There are two hydrogen adsorption pathway on CNTs. First is the physical adsorption of hydrogen molecules, which is favored

at high H₂ pressure atmosphere. The other way is electrochemical adsorption of hydrogen, which is applicable to secondary batteries that are beneficial for configuring small-scale energy storage systems.¹⁵ Electrochemical hydrogen storage provides high capacity at ambient temperature and atmospheric pressure than conventional hydrogen storage technology at low temperature and high pressure.¹⁶

Metals mainly Ni, Ag, Pd and Pt. or metal oxides such as TiO₂ nanocatalysts decorated on CNTs lead to increase in its hydrogen storage through a very interesting mechanism called spillover mechanism.^{7,13,17-20} Metal or metal oxides nanoparticles spill hydrogen over the carbon nanotubes and when their highest content exposed to hydrogen during the adsorption process, spillover mechanism is achieved.^{19,21}

Moreover, bimetallic catalyst nanostructures are favorable as sustainable energy technology and are good choice for achievement of selectivity, stability and superior specific activity in various applications such as catalysis,^{22,23} chemical/gas sensors,²⁴ fuel cells,^{25,26} hydrogen generation,²⁷ and hydrogen storage,²⁸⁻²⁹ compare to their monometallic counterparts. On the other hand, the addition of the second metal may cause considerable changes in catalytic properties, activity and selectivity.²³

Palladium and platinum and their bimetallic systems are a class of interesting materials for storing hydrogen due to their fast adsorption/ desorption rates which their application for hydrogen storage because of their expensive and high cost is restricted.^{17,29-31}

^a Chemistry Department, Yasouj University, Yasouj 75918-74831, Iran.

^b Electrical & Computer Engineering Department, North Carolina State University, Raleigh, NC 27606, USA.

*Corresponding author: Tel: +98 741 2223048; Fax: +98 741 2223048
E-mail address: m_ghaedi@mail.yc.ac.ir; m_ghaedi@yahoo.com M. Ghaedi.

The conspicuous physiochemical catalytic properties, strong structural characteristic and relatively low cost of silver make it noteworthy materials for hydrogen storage. Silver can combine with some other metals such iron and form bimetallic systems.^{32,33} The effect of iron on improving the effective storing capacity of some hydrogen storage materials such alloys was investigated.^{34,35} Particularly, the bimetallic Fe-Ag particles exhibited a higher hydrogen storage compared to the monometallic Fe or Ag particles. The increase in storage capacity was attributed to the strong metal-metal interaction which enhances hydrogen spillover effect by adjustment of the electronic structure of Ag using Fe. The size and surface site distribution of particles have a significant influence on the electrochemical response of hydrogen at hydrogen storage materials.^{29,36,37}

Fast hydrogen diffusion in nanostructured materials significantly improves the kinetics of hydrogen absorption and desorption.³⁸⁻⁴⁰

Therefore, CNTs decorated via bimetallic materials expected to have the ability for electrochemical hydrogen storage.^{29,31}

Additionally, metal oxides are attractive, low toxicity and economical energy storage materials for electrochemical capacitor applications.¹⁹ Among the metal oxides, TiO₂ with anatase and ⁴¹ rutile ⁴² phases have attracted much interest and is a promising material for energy storage because of its excellent charge storage capability, high redox activity, low cost and superior electrochemical properties.^{43,44} To date, the various composite has been developed based on TiO₂ and conductive components such as carbon nanotubes CNTs, graphene and carbon black.⁴⁵⁻⁴⁷ Research results demonstrate that TiO₂ nanocatalyst coated CNTs have better electrochemical storage performance which enhances more hydrogen storage capacity than the pure CNTs.^{45,48,49}

Inspired by these findings, tried to use low cost and effective materials with a high capacity for hydrogen storage. In this work, Fe-Ag/CNTs nanocomposite with high hydrogen storage capacity was prepared by coating nanoporous bimetallic Fe-Ag nanoparticles, which were synthesized by a simple chemical reduction method, on the surface of oxidized MWCNTs. Moreover, the nanoporous bimetallic Fe-Ag/TiO₂ nanoparticles with different amounts of Fe-Ag NPs were synthesized using a facile hydrothermal method and subsequently the effect of TiO₂ nanoparticles on the improvement of hydrogen storage capacity of Fe-Ag/CNTs nanocomposites were optimized. The absence of any report on the application of the nanoporous bimetallic Fe-Ag/TiO₂ nanoparticles decorated on the surface of CNTs for hydrogen storage encourages our group to focus on this subject. The key finding of the present study is attention for finding the best composition of bimetallic Fe-Ag/TiO₂ nanoparticles which lead to significant improvement in their efficiency for hydrogen storage. Our studies have shown that the nanoporous bimetallic Fe-Ag/TiO₂ nanoparticles decorated on the surface of MWCNTs with the best composition of 0.04 M Fe-Ag nanoparticles significantly enhance hydrogen storage capacity.

2. Experimental

The chemicals used in this investigation were iron(III) nitrate nonahydrate (Fe(NO₃)₃·9H₂O), silver nitrate (AgNO₃), tri-sodium citrate, titanium isopropoxide (TTIP) and multi-walled carbon nanotubes (MWCNTs, outer diameter 10-20 nm, length 20 μm) purchased from Sigma-Aldrich. Polyvidone 25, sodium borohydride (NaBH₄) and acetic acid were procured by Merck. Absolute ethanol and deionized water were used during the preparation of powders. All the chemicals were used without further purification.

2.1. Materials characterization

The powder X-ray diffraction XRD patterns of the products were determined using a Phillips X' Pert PRO equipped with a Cu Kα source having a scanning range of 0–80 Bragg's angle. The morphologies characterization was obtained by using a Philips XL-30FESEM field emission scanning electron microscopy (FESEM) equipped with an energy dispersive X-ray analyzer (EDS). Elemental distribution of the samples was revealed using a HAADF-STEM-FEI Titan 80-300 high angle annular dark-field scanning transmission electron microscopy (HAADF-STEM) equipped with EDS. The EDS spectroscopy and elemental mapping were used for compositional analysis and to investigate the homogeneity of the elemental distribution. The Raman spectrum was measured with a Takram P50COR10 Teksan Dispersive Raman Spectrometer equipped with a 532 nm Nd:YLF laser as the excitation source.

2.2. Preparation of nanoporous bimetallic Fe-Ag nanoparticles and Fe-Ag/CNT nanocomposite

The nanoporous bimetallic Fe-Ag NPs was prepared as follow: 5 mL of 0.02 M Fe(NO₃)₃·9H₂O, 5 mL 0.034 M tri-sodium citrate and 10 mL 0.5 g polyvidone 25 which all dissolved in de-ionized water, were diluted by 20 mL of de-ionized water. The mixed solution was stirred for 15 min at ambient temperature under an argon atmosphere and subsequently 0.3 g sodium borohydride in 20 mL de-ionized water was added drop-wise. After 1 h stirring, 5 mL of 0.01 M AgNO₃ and 10 mL of sodium borohydride solution (0.2 g NaBH₄) were added drop-wise into the above solution. After 2 h of stirring, the obtained colloidal solution was centrifuged at 12000 rpm for 10 min and washed several times with de-ionized water and absolute ethanol and its pH was adjusted to 7. The final product was dried in a vacuum oven overnight at 50 °C for 24 h.

The Fe-Ag/CNT nanocomposite was prepared by reduction of Fe(NO₃)₃·9H₂O and AgNO₃ precursors and loaded onto oxidized MWCNTs suspension. A chemical oxidation method was used to implant various oxygen containing onto the MWCNTs according to the literature.⁵⁰ First, 0.04 g of oxidized MWCNTs were mixed with 5 mL of 0.02 M Fe(NO₃)₃·9H₂O solution and stirred under air atmosphere for 2 h. The following process was performed as

described above, just after adding the additional sodium borohydride solution, the mixture was stirred for 24 h.

2.3. Preparation of nanoporous bimetallic Fe-Ag/TiO₂ nanoparticles and Fe-Ag/TiO₂/CNT nanocomposites

In typical procedure, 2 mL of the above-described nanoporous bimetallic Fe-Ag NPs with the concentrations of 0.01, 0.04 and 0.1 M were dispersed in 30 mL absolute ethanol for 15 min and then 1 mL of acetic acid was added and sonicated for another 30 min. In next step, 0.2 mL of TTIP was added dropwise into the above mixture and after 1 h stirring at room temperature, the suspension was transferred into a Teflon-lined autoclave which was sealed and heated at 150 °C for 12 h. After cooling to room temperature, this solution was centrifuged at 7000 rpm for 10 min. The precipitate washed with deionized water and absolute ethanol once more. Finally, the bimetallic Fe-Ag/TiO₂ NPs were dried in air at 80 °C for 12 h and their products labeled as (0.01)Fe-Ag/TiO₂, (0.04)Fe-Ag/TiO₂ and (0.1)Fe-Ag/TiO₂.

The typical process utilized for supporting the oxidized carbon nanotubes with nanoparticles. 2 mg of oxidized MWCNTs were dispersed in 20 ml deionized water under sonication for 30 min to prepare a colloidal suspension of CNTs. Then, 2 mg of as-prepared bimetallic Fe-Ag/TiO₂ nanoparticles were added to the scattered solution and dispersed for 24 h. Finally, the products were collected by centrifugation, washed with deionized water and absolute ethanol three times and dried at 80 °C for 12 h.

2.4. Preparation of working electrodes

Copper foam with nano-sized pores was washed with acetone and deionized water and subsequently dried under vacuum condition at 70 °C for 2 h. The as-prepared nanocomposites were ultrasonically dispersed in 1 mL of 1:1 v/v deionized water:2-propanol and a few drops of Nafion 0.5 wt% mixture for 30 min. Then, a pure copper foam with a surface area of 1×1 cm² was coated with a thin layer of a sonicated solution of the sample at 100 °C.

2.5. Electrochemical measurements

Sama 500 potentiostat electrochemical workstation Isfahan, Iran equipped with the three-electrode system was employed for electrochemical studies at ambient temperature and pressure in 6.0 M KOH aqueous solution. The platinum plate and the Ag/AgCl were used as the counter and reference electrodes, respectively. For charging/ discharging experiments, the prepared working electrodes were fully charged at a current density of 11000 mA g⁻¹ for 30 min followed by 5 min rest and then discharged at 4000 mA g⁻¹. The discharge cell potential cutoff was set to 0.34 V.

Cyclic voltammetry (CV) measurement of the working electrodes was done in a potential range of -1.2 to 0 V vs. Ag/AgCl electrode at a scan rate of 100 mV s⁻¹.

3. Results and discussion

The phase and purity of the samples were confirmed by powder X-ray diffraction (XRD). Fig. 1a shows XRD pattern of nanoporous bimetallic Fe-Ag NPs which is composed of few sharp diffraction peaks appeared at 2θ value ca. 38.2°, 44.6°, 64.7° and 77.7°, which corresponds to the (111), (200), (220) and (311) crystal planes of the face-centered-cubic (fcc) silver (JCPDS No.87-0717), respectively. The two distinct peaks at 44.6° and 64.7° steadily assigned to the characteristic (110) and (200) diffractions of fcc iron (JCPDS No.01-1262) but the Ag-peaks prevailed over Fe-peaks. The nonobservance of iron peaks in the bimetallic sample which has about 57% of iron is may be due to Fe particles which are surrounded by Ag atoms and further confirm by FESEM and STEM images. It is obvious that there was no significant peak shift, representing the Fe and Ag phase separation as well as the non-existence of Fe-Ag alloy.

Fig. 1 also depicts XRD patterns for the bimetallic Fe-Ag/TiO₂ nanoparticles synthesized with different concentrations of bimetallic Fe-Ag NPs which display typical characteristic peaks for anatase TiO₂ JCPDS (No.04-0477). The diffraction peaks of (004) crystal plane of anatase TiO₂ and (111) plane of Ag were overlapped with each other. The XRD profile of (0.01)Fe-Ag/TiO₂, as seen is without peaks related to Fe and Ag (Fig. 1b), that may be due to the low concentration and high dispersion of metal species on TiO₂ surface.⁵¹ Increasing the concentration of Fe-Ag NPs lead to the appearance of characteristic peaks assigned to the presence of metals, as observed in the XRD patterns of (0.04)Fe-Ag/TiO₂ (Fig. 1c) and (0.10)Fe-Ag/TiO₂ (Fig. 1d). No additional peaks belong to impurity phase in all XRD patterns indicate the high purity of the obtained samples.

As calculated from the full width at half-maximum (FWHM) of the (101) reflection peaks, the average crystallite sizes of bimetallic (0.01)Fe-Ag/TiO₂, (0.04)Fe-Ag/TiO₂ and (0.1)Fe-Ag/TiO₂ samples are 14.2, 9.3 and 10.4 nm, respectively, according to Scherrer's formula ($D=0.89 \lambda/\beta \cos \theta$), where D, λ, θ and β are respectively the averaged dimension of crystallites, wavelength of the CuKα₁ radiation (0.1541 nm) and the Bragg angle of the peak and the FWHM of peak in radians. It is clearly seen that the smallest average particle size related to Fe-Ag/TiO₂ nanoparticles with the 0.04 M of bimetallic Fe-Ag NPs. The reduced particle size cause increasing surface area and extensively enhance its ability for adsorption of hydrogen.

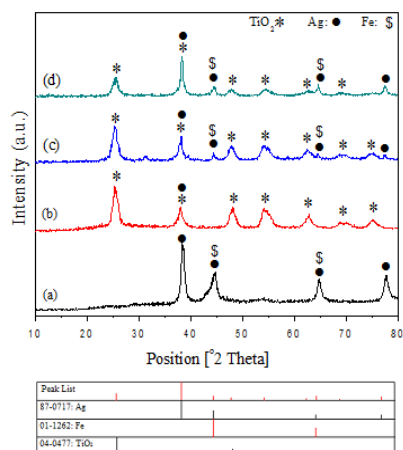


Fig. 1 The XRD patterns of bimetallic (a) Fe-Ag (b) (0.01)Fe-Ag/TiO₂ (c) (0.04)Fe-Ag/TiO₂ (d) (0.1)Fe-Ag/TiO₂ nanoparticles.

The XRD patterns of bimetallic Fe-Ag and Fe-Ag/TiO₂ nanoparticles decorated on the surface of MWCNTs were given in Fig. 2A. The peak appeared at around $2\theta = 26.3^\circ$, belong to (002) is corresponding to the MWCNTs which was overlap with the intense peak of anatase TiO₂ (101) in Fe-Ag/TiO₂ NPs decorated on MWCNTs samples. As can be seen in Fig. 2A, the XRD patterns of Fe-Ag/CNT and Fe-Ag/TiO₂/CNT nanocomposites are almost identical to that of bimetallic Fe-Ag and Fe-Ag/TiO₂ (Fig. 1), respectively which confirm the absence of significant change in a structure following their loading on MWCNTs. No apparent impurity phase is observed in all XRD patterns.

The structure and crystallinity of Fe-Ag/CNT, (0.01)Fe-Ag/TiO₂/CNT, (0.04)Fe-Ag/TiO₂/CNT and (0.1)Fe-Ag/TiO₂/CNT nanocomposites was further analyzed using Raman spectroscopy (Fig. 2B) and summary of the results are shown in table 1. The typical Raman active modes of anatase TiO₂ (D_{4h} point group) are composed of four peaks at the low-frequency region around 147 (E_g), 395 (B_{1g}), 514 (B_{1g}) and 636 cm⁻¹ (E_g). It can be deduced that all constructed samples are assigned to the anatase phase and without any pieces of evidence for the presence of rutile phase which has good agreement with the XRD studies.

In general, the D (1350 cm⁻¹) and G (1585 cm⁻¹) bands which are characteristic of graphite based carbons⁷ are observed in all the experiments. The D band is mainly due to the presence of sp³ defects induced disordering in carbon systems and G band is related to the vibration of sp²-bonded carbon atoms of graphite.⁵² The peak at 2633 cm⁻¹ corresponds to the second harmonic of the D (G' or 2D) peak. I_D/I_G intensity ratio of the peaks is used as a rough measure of the sample quality.⁵³ The slight increase of I_D/I_G ratio implied more defects are formed due to the presence of TiO₂ in Fe-Ag/TiO₂/CNT nanocomposites. Meanwhile, the high I_D/I_G ratio is suggestive of a defect in carbon structure which can facilitate the diffusion of H⁺ ions through the disordered region. On the other hands, the created defects facilitate the spillover of hydrogen from nanoporous bimetallic Fe-Ag/TiO₂ nanoparticles to carbon nanotubes. The

increase in the quality of the bimetallic (0.04)Fe-Ag/TiO₂ nanoparticles decorated on MWCNTs in comparison to two other samples indicates that structure appeared in the presence of 0.04 M bimetallic Fe-Ag NPs lead to the destruction of MWCNTs structures. Therefore, the preparation of well-suited Fe-Ag/TiO₂/CNT nanocomposite with the appropriate amount of nanoporous bimetallic Fe-Ag NPs is crucial.

Table 1

List of the vibrational frequencies (cm⁻¹) derived from the Raman spectra.

samples	TiO ₂ peak position (cm ⁻¹)	D band (cm ⁻¹)	G band (cm ⁻¹)	I _D /I _G
Fe-Ag/CNT	-	1344	1561	0.75
(0.01)Fe-Ag/TiO ₂ /CNT	147,391,507,620	1344	1561	0.81
(0.04)Fe-Ag/TiO ₂ /CNT	147,391,501,620	1342	1557	0.88
(0.1)Fe-Ag/TiO ₂ /CNT	147,389,519,626	1343	1561	0.85

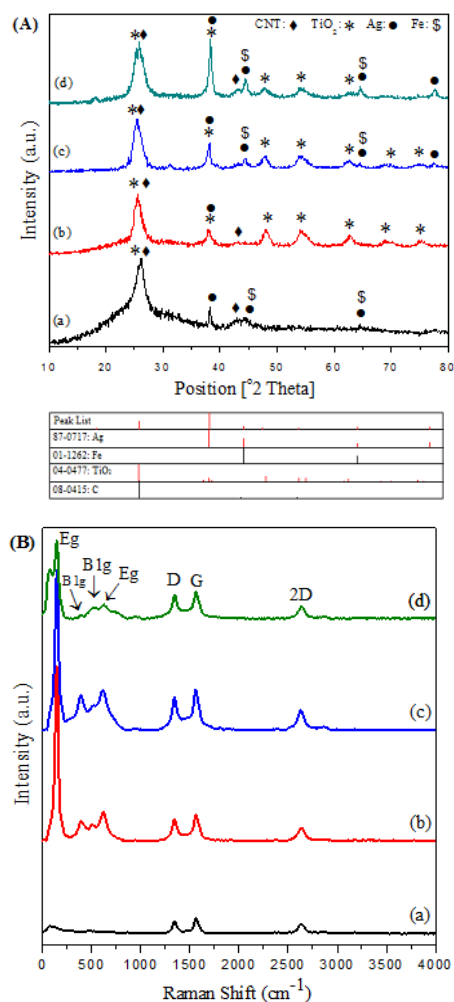


Fig. 2 (A) The XRD patterns and **(B)** Raman spectra of (a) Fe-Ag/CNT (b) (0.01)Fe-Ag/TiO₂/CNT (c) (0.04)Fe-Ag/TiO₂/CNT (d) (0.1)Fe-Ag/TiO₂/CNT nanocomposites.

Fig. 3A and B represent typical FESEM images of the nanoporous bimetallic Fe-Ag NPs which approximately confirm its nanoporous and homogeneous string structures which consist of irregular pores with several nanometers in diameter. These results are explained based on surrounding the large scale Fe nanoparticles by small size Ag nanoparticles that create nanoporous morphology which is proportional to supplying large surface area which is highly required for hydrogen adsorption. The EDS line profile (Fig. 3C) suggests that bimetallic Fe-Ag structure consists of two parts, one rich in Fe (57 %) and another one rich in Ag (43 %).

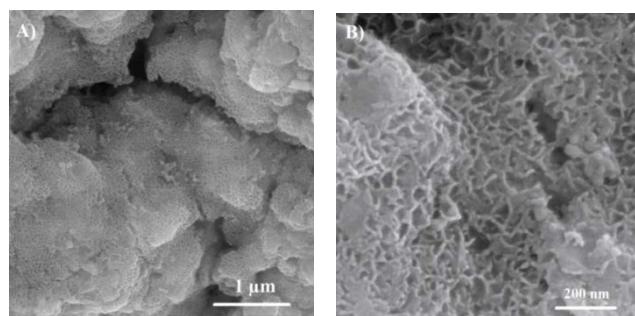


Fig. 3 (A) and (B) FESEM images and (C) EDS line profile of nanoporous bimetallic Fe-Ag nanoparticles.

High angle annular dark-field scanning transmission electron microscopy (HAADF-STEM) was successfully applied to further characterize the morphology and elemental distribution of nanoporous bimetallic Fe-Ag nanoparticles. Fig. 4 clearly shows that the Fe nanoparticles with an average particle size of 25–35 nm are surrounded by a large number of very small Ag atoms that create a porous structure. The elemental mapping images revealed the segregation of the Fe and the Ag particles together without their alloying phenomenon.

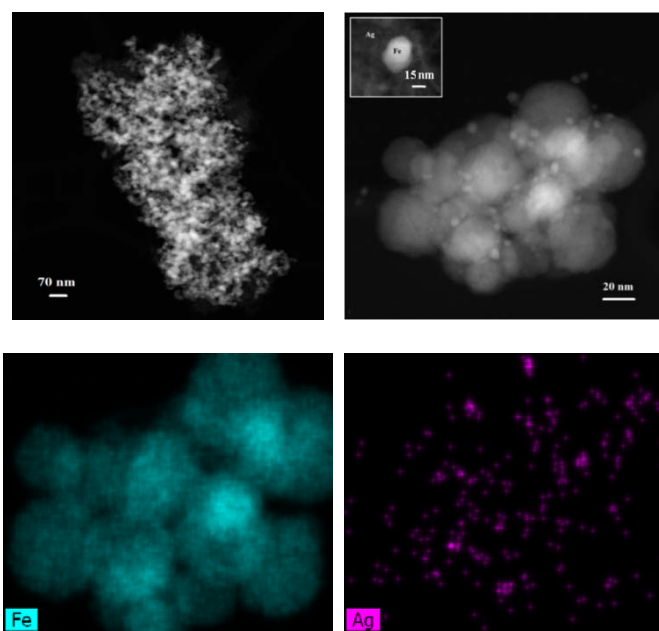


Fig. 4 STEM and elemental mappings images of nanoporous bimetallic Fe-Ag nanoparticles.

The FESEM images and particle size distribution, according to digimizer software, of bimetallic Fe-Ag/TiO₂ nanoparticles synthesized with different concentrations of bimetallic Fe-Ag NPs are shown in Fig. 5. The bimetallic (0.01)Fe-Ag/TiO₂ sample is comprised of aggregated particles with low homogeneity. Increasing content of bimetallic Fe-Ag NPs from 0.01 to 0.04 and 0.1 lead to the formation of uniform particles size and morphology. The bimetallic (0.04)Fe-Ag/TiO₂ sample is composed of separate and free aggregate nanoparticles (Fig. 5C) with average particle size in the range of 8 to 10 nm in comparison with 14–16 nm for (0.01)Fe-Ag/TiO₂ and 8–12 nm for (0.1)Fe-Ag/TiO₂ which consistent with the results of XRD. The porous structure and reduction in particle size lead to increase in surface area which is desirable for hydrogen sorption and storage. The EDS line profile as shown in Fig. 5G, strongly evidences that the elements are Fe, Ag, Ti and O. The surface morphology of the nanoporous bimetallic (0.04)Fe-Ag/TiO₂ nanoparticles decorated on the surface of MWCNTs were examined by FESEM as shown in Fig. 6A which strongly denote uniform formation of nanoparticles and its well-dispersion on the external wall of the MWCNTs with spherical morphology. The average particle size is 8.0–10 nm by measuring more than 100 nanoparticles. The high dispersion of bimetallic Fe-Ag/TiO₂ nanoparticles on the MWCNTs surface is one of the most important reasons for the improvement of hydrogen storage capacity. As shown in Fig. 6B, the EDS line profile exactly confirms the existence of Fe, Ag, Ti, O and C elements. Furthermore, the distribution of nanoparticles on the surface of MWCNTs was analyzed by elemental mappings (Fig. 7). The results clearly reveal well deposition of Fe, Ag and TiO₂ nanoparticles on the surface of MWCNTs.

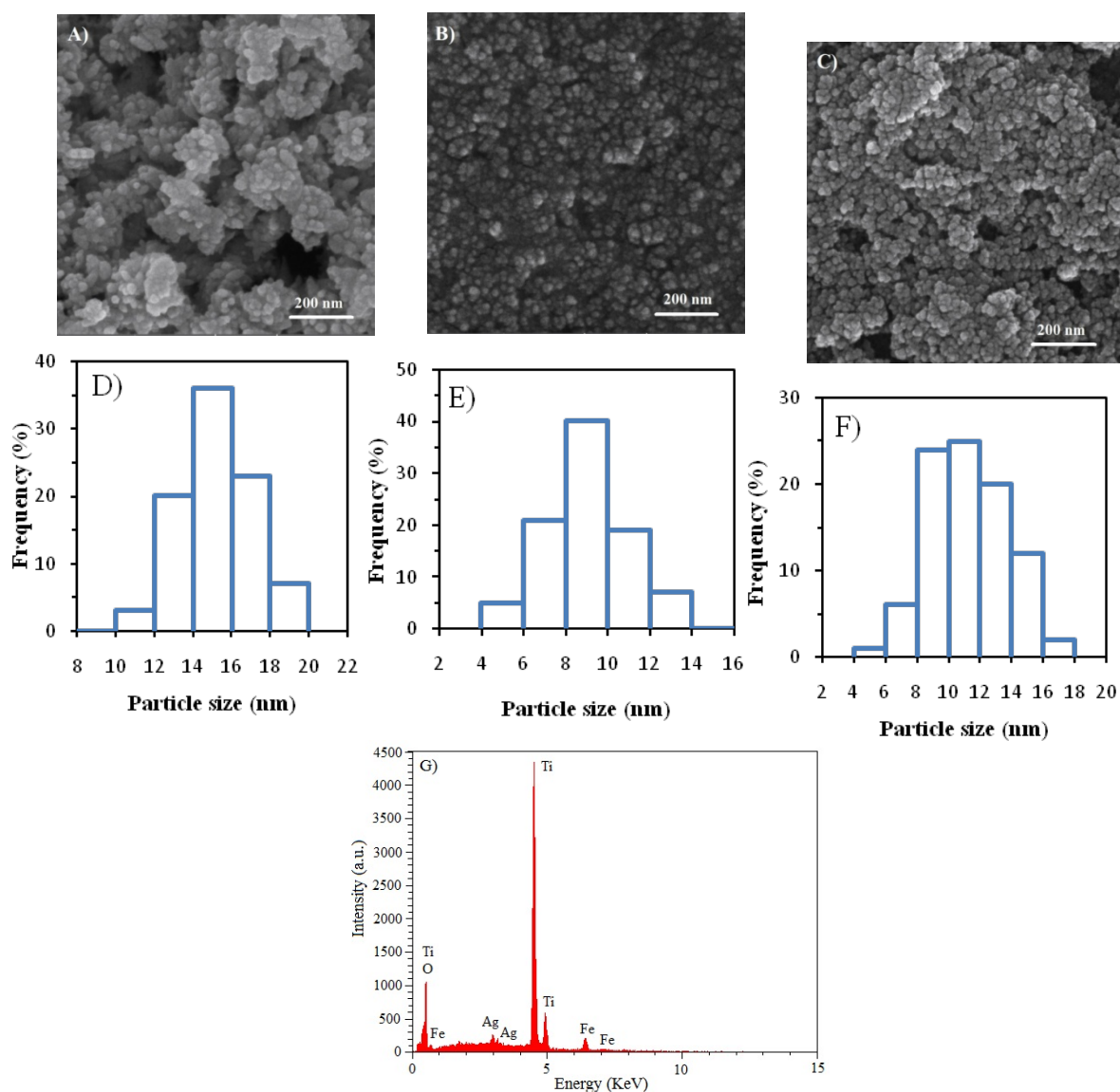


Fig. 5 FESEM images and particle size distribution of bimetallic nanoparticles: (A) and (D) (0.01)Fe-Ag/TiO₂; (B) and (E) (0.04)Fe-Ag/TiO₂; (C) and (F) (0.1)Fe-Ag/TiO₂. (G) EDS analysis of (0.04)Fe-Ag/TiO₂ sample shown in (B).

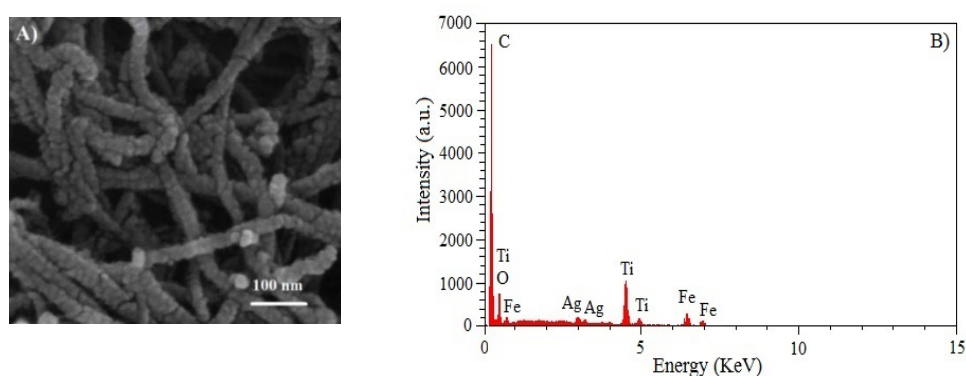


Fig. 6 (A) FESEM and (B) EDS line profile of nanoporous bimetallic (0.04)Fe-Ag/TiO₂ nanoparticles decorated on the surface of MWCNTs.

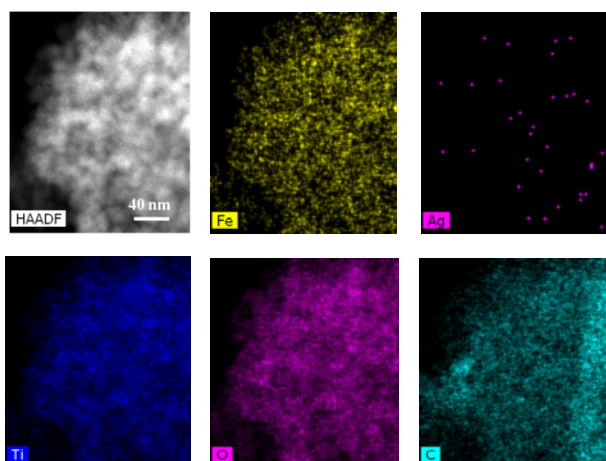


Fig. 7 Elemental mappings images of nanoporous bimetallic (0.04)Fe-Ag/TiO₂ nanoparticles decorated on the surface of MWCNTs.

The schematic synthetic process for the preparation of Fe-Ag/TiO₂ nanoparticles decorated on the surface of MWCNTs is shown in Fig. 8.

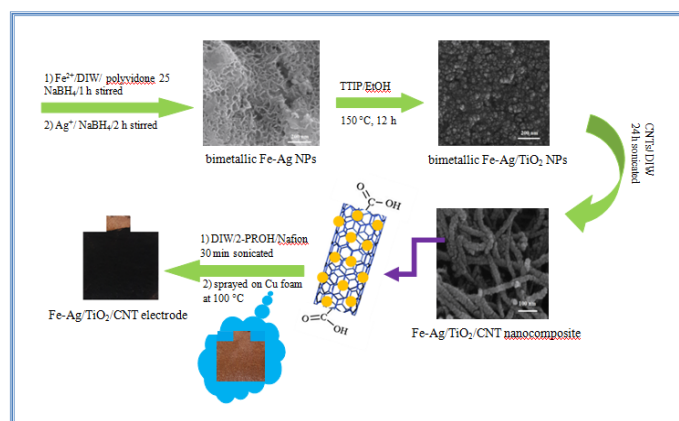


Fig. 8 Schematic illustrated the synthesis of the Fe-Ag/TiO₂/CNT electrode.

To explore the electrochemical hydrogen storage performance of the as-prepared nanocomposites, a three-electrode cell in a 6 M KOH solution was assembled (see experiment section for details) and the charge and discharge curves were recorded as shown in Fig. 9A and B. The amount of hydrogen stored is calculated according to the following measurement of released hydrogen from various samples and respectively their discharge capacities are listed in Table 2. The discharge capacity of copper foam before the coating is less than 1 mAh g⁻¹ (Fig. 9C) which proof low and negligible contribution of copper foam for a discharge capacity of the samples.

As shown in Fig. 9B, the discharging capacity of Fe-Ag/CNT electrode is 1103 mAh g⁻¹ which is higher than that of the Ag/CNT electrode (845 mAh g⁻¹) which probably is related to strong electronic interactions between Fe and Ag which significantly boost the hydrogen electroadsorption properties of Ag.

It is clearly seen in Fig. 9B that the presence of TiO₂ in Fe-Ag/CNT nanocomposite has a significant influence on the improvement of spillover phenomenon and discharge capacity of the samples. TiO₂ nanoparticles have outstanding redox ability and serve as a catalyst, which can enhance the reduction of H⁺ and the oxidation of H atoms.⁵⁴ The discharging capacity for (0.1)Fe-Ag/TiO₂/CNT electrode is higher than that of (0.01)Fe-Ag/TiO₂/CNT but lower than that of (0.04)Fe-Ag/TiO₂/CNT. The maximal discharge capacity of 2931 mAh g⁻¹ was obtained for the (0.04)Fe-Ag/TiO₂/CNT electrode which is higher than that of other two electrodes. It was noteworthy that the higher Fe-Ag content can wall up the channels of the MWCNTs and reduce the effective positions for the adsorption of the H⁺ ions on MWCNTs. Thus, by preventing from hydrogen entrance into the tube, lead to lower discharging capacity.

Besides, it can be deduced that the hydrogen storage capacity of (0.04)Fe-Ag/TiO₂/CNT electrode was 10.94 wt% which improved nearly by 499% for hydrogen storage capacity in comparison to pristine MWCNTs. The enhancement of about 5 times is due to the interfacial diffusion of hydrogen from Fe-Ag/TiO₂ nanoparticles to the carbon nanotube surface. Furthermore, as shown in the Fig. 9B, the discharging voltage plateau was observed at about 0.46 V and 0.48 V, respectively, while for the Fe-Ag/TiO₂/CNT electrodes the discharging voltage plateau was shown at 0.58 V.

As a result, TiO₂ nanoparticles can significantly improve the adsorption of hydrogen atoms on the surface of Fe-Ag/CNT nanocomposite. The results reveal that by controlling the content of nanoporous bimetallic Fe-Ag NPs, the Fe-Ag/TiO₂/CNT nanocomposites reach the highest discharge capacity promptly. The Fe-Ag/TiO₂/CNT nanocomposite with the optimum composition of 0.04 M bimetallic Fe-Ag NPs significantly enhances the hydrogen storage capacity of MWCNTs from 2.19 wt% to 10.94 wt%. Fig. 9D and E show the cycle life and stability for electrochemical hydrogen storage of (0.04)Fe-Ag/TiO₂/CNT electrode. A high and stable discharge capacity of 11108 mAh g⁻¹ is achieved after 20 cycles which are quite interesting for the battery applications in comparison to other materials.^{29,17,48,55} This finding exhibits an excellent cycle stability and a high degree of electrochemical reversibility in the repetitive charge/ discharge tests.

Table 2

The discharge and H₂ storage capacities of the different nanocomposites.

Sample	Discharge capacity mAh g ⁻¹	H ₂ storage wt%
CNTs	587	2.19
Ag/CNT	845	3.15
Fe-Ag/CNT	1103	4.12
(0.01)Fe-Ag/TiO ₂ /CNT	1621	6.05
(0.04)Fe-Ag/TiO ₂ /CNT	2931	10.94
(0.1)Fe-Ag/TiO ₂ /CNT	1976	7.37

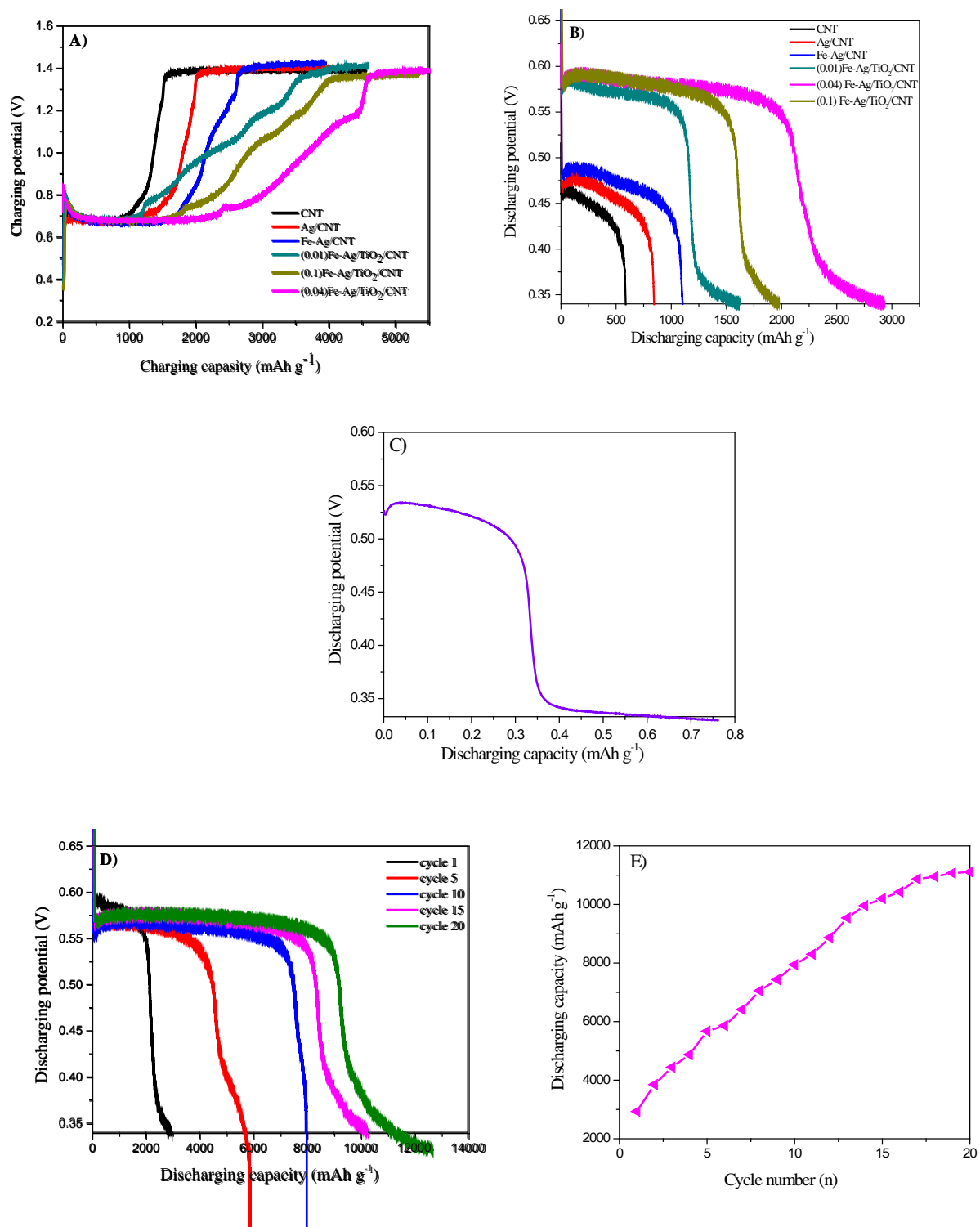


Fig. 9 (A, B) Discharge curves of pristine CNTs, Ag/CNT, Fe-Ag/CNT, (0.01)Fe-Ag/TiO₂/CNT, (0.04)Fe-Ag/TiO₂/CNT and (0.1)Fe-Ag/TiO₂/CNT electrodes; (C) discharge capacity curve of copper foam in the absence of nanocomposites; (D) and (E) cycle performance of (0.04)Fe-Ag/TiO₂/CNT electrode.

Cyclic voltammogram (CV) curves were recorded to investigate the electrochemical hydrogen adsorption/ desorption behavior of the Fe-Ag/CNT and (0.04)Fe-Ag/TiO₂/CNT electrodes as shown in Fig. 10. In the cathodic direction, one broad reduction peak of hydrogen is clearly observed at the potential of -0.95 V, generally correspond to the electrochemical hydrogen adsorption on the surfaces of Fe-Ag/TiO₂/CNT electrode, while for the Fe-Ag/CNT sample the peak is around -1.0 V.^{9,48,56}

During the reverse scan, the anodic current peak is appeared around -0.5 V and -0.44 V potential for the Fe-Ag/TiO₂/CNT and Fe-Ag/CNT electrodes, respectively, which related to the electrochemical desorption of hydrogen atom adsorbed on the surfaces of the electrode material.^{9,57} It can be deduced from the curves that introducing TiO₂ into the Fe-Ag/CNT nanocomposite lead to movement of the cathodic reduction and anodic oxidation peaks to the positive and negative potential direction, respectively.

These results indicate more easily oxidation of H atoms and reduction of H⁺ which could be contributed to the preferable redox ability of TiO₂ nanoparticles. Moreover, shifting the oxidation peaks to the negative value suggests a strong chemisorption of hydrogen (atomic hydrogen bonded to CNTs).⁵⁸

Furthermore, the considerable increase of the current density of the hydrogen adsorption/ desorption peaks implies that the presence of TiO₂ NPs improves the electrochemical hydrogen storage capacity of Fe-Ag/CNT.

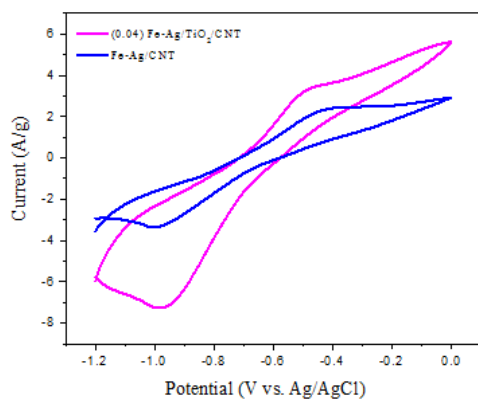
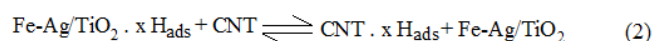
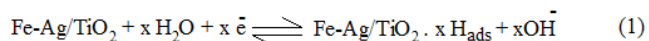


Fig.10 Cyclic voltammogram curve of the Fe-Ag/CNT and (0.04)Fe-Ag/TiO₂/CNT electrodes.

Based on the above discussion, the mechanism of the electrochemical hydrogen storage process of the Fe-Ag/TiO₂/CNT nanocomposite electrodes can be explained as follows.^{59,48}



Bimetallic Fe-Ag nanoparticles can act as redox sites for hydrogen storage which enhance the spillover effect and thereby increase the electrochemical hydrogen adsorption on the surfaces of MWCNTs. Moreover, the high redox activity of TiO₂ NPs is profitable for the decomposition of water molecules

and the reduction of H⁺ on the charging process and oxidation of H atoms when the electrode is in the discharging status. The presence of TiO₂ on the surface of Fe-Ag/CNT nanocomposite enhances the surface area for hydrogen adsorption. Thus the faster electron transfer and the larger surface area provides more active sites for the adsorption of hydrogen and supply greater electrochemical hydrogen storage capacity.⁵⁴

The comparison of hydrogen storage capacity between the (0.04)Fe-Ag/TiO₂/CNT nanocomposite correspond to present research with other reported hydrogen storage materials is reported in table 3 which strongly support first application for hydrogen storage capacity of Fe-Ag/TiO₂/CNT nanocomposite under electrochemical process while has high hydrogen storage capacity and can deliver comparable performance in comparison to recent hydrogen storage materials. As previously mentioned, the electrochemical hydrogen storage is very valuable method which provides more capacity than common hydrogen storage technology at low temperature and high pressure.⁶⁰

Table 3

Hydrogen storage capacity of different reported materials.

S. No	Materials used	Hydrogen storage method	H ₂ storage wt%	Reference
1	Fe-doped MWCNTs	electrochemical	1.90	53
2	Pd-decorated CNTs	moderate pressure	H ₂ 4.50	61
3	CNTs	pressure	6.07	13
4	Ni-supported MWCNTs	electrochemical	1.27	21
5	Ni coated MWCNTs	moderate pressure	H ₂ 2.62	56
6	Co coated MWCNTs	electrochemical		
7	MWCNTs	moderate pressure	H ₂ 2.30	62
8	coated Pd-Ni MWCNTs	pressure	2.00	17
9	MWCNTs decorated Pt-Pd	moderate pressure	H ₂ 1.79	63
10	decorated Pt-Pd MWCNTs	pressure		
11	TiO ₂ -decorated CNTs	electrochemical	2.02	48
12	Fe-Ag/TiO ₂ /CNT	electrochemical	10.94	This paper

4. Conclusions

In summary, a novel nanocomposite structure with high hydrogen storage capacity was prepared based on the deposition of nanoporous bimetallic Fe-Ag nanoparticles on the surface of oxidized MWCNTs. TiO₂ nanoparticles with high redox ability were used as supplementary adsorbents so that the amount of the total adsorbed hydrogen enhanced

significantly. The presence of TiO₂ on the surface of Fe-Ag/CNT nanocomposite increased the surface area and stimulated the Fe-Ag/CNT reaching a large discharge capacity and significantly improved electrochemical hydrogen storage. Moreover, the capacity for the hydrogen sorption and storage depended strongly on the content of bimetallic Fe-Ag nanoparticles. It was found that the Fe-Ag/TiO₂/CNT nanocomposite consisting 0.04 M of bimetallic Fe-Ag NPs can supply up to 2931 mAh g⁻¹ discharging capacity corresponding to 10.94 wt% hydrogen storage capacity, which is by far the highest value among the reported CNTs electrodes. It is notable that after 20 cycles, the capacity increased by 379%, with an excellent cycle stability, which is highly promising for applications in the secondary hydrogen batteries. The demonstrated hydrogen storage capacity is both large and affordable due to the low-cost of the primary materials and the methods involved in this process. As a result, the electrochemical process of adsorption/ desorption of hydrogen in carbon materials decorated with transition metals in bimetallic form and transition metal oxides as catalysts is recommended as a hydrogen storage method for the future.

Conflicts of interest

There are no conflicts to declare

Acknowledgements

This study is based upon work supported partially by Research Council of the Yasouj University, the Protection of Researchers and Technology under grant number 96005467, the National Science Foundation under grant numbers ECCS-1351533, and CMMI-1363485 and AFOSR under contract number FA9550-12-1-0225.

References

- Z. Wang, Z. Shi, Z. Gu, *Carbon*, 2010, **48**, 443–446.
- Z. M. Ao, F. M. Peeters, *Physical Review, B* 2010, **81**, 205406.
- E. L. Gonzalez, F. I. Llerena, M. S. Perez, F. R. Iglesias, J. G. Macho, *International Journal of Hydrogen Energy*, 2015, **40**, 5518-5525.
- Y. Wu, X. Jiang, J. Chen, Y. Qi, Y. Zhang, H. Fu, J. Zheng, X. Li, *Dalton Transactions*, 2017, **46**, 4499-4503.
- N. N. Sulaiman, M. Ismail, *Dalton Transactions*, 2016, **45**, 19380-19388.
- L. Z. Ouyang, W. Chen, J. W. Liu, M. Felderhoff, H. Wang, M. Zhu, *Advanced Energy Materials*, 2017, 1700299.
- W. Chen, L. Z. Ouyang, J. W. Liu, X. D. Yao, H. Wang, Z. W. Liu, M. Zhu, *Journal of Power Sources*, 2017, **359**, 400-407.
- H. Zhong, L. Z. Ouyang, J. S. Ye, J. W. Liu, H. Wang, X. D. Yao, M. Zhu, *Energy Storage Materials*, 2017, **7** 222-228.
- L. Han, W. Qin, J. Jian, J. Liu, X. Wu, P. Gao, B. Hultman, G. Wu, *Journal of Power Sources*, 2017, **358**, 93-100.
- L. Z. Ouyang, Z. J. Cao, H. Wang, R. Hu, M. Zhu, *Journal of Alloys and Compounds*, 2017, **691**, 422-435.
- C. Lin, L. Yang, L. Z. Ouyang, J. W. Liu, H. Wang, M. Zhu, *Journal of Alloys and Compounds*, 2017, **728**, 578-584.
- L. Z. Ouyang, Z. J. Cao, L. L. Li, H. Wang, J. W. Liu, D. Min, Y. W. Chen, F. M. Xiao, R. H. Tang, M. Zhu, *International journal of hydrogen energy*, 2014, **39**, 12765-12772.
- R. Naresh Muthu, S. Rajashabala, R. Kannan, *Renewable Energy*, 2016, **85**, 387-394.
- H. Nishihara, T. Kyotani, *Advanced Materials*, 2012, **24**, 4473-4498.
- R. Akbarzadeh, H. Dehghani, *Journal of Solid State Electrochemistry*, 2018, **22**, 395–405
- L. Zhou, X. Qu, D. Zheng, H. Tang, D. Liu, D. Qu, Z. Xie, J. Li, D. Qu, *ACS appl. Mater. Interfaces*, 2017, **47**, 41332.
- S. W. Hwang, S. U. Rather, M. U. D. Naik, C. S. Soo, K. S. Nahm, *Journal of Alloys and Compounds*, 2009, **480**, 20–24.
- L. Han, W. Qin, J. Zhou, J. Jian, S. Lu, X. Wu, G. Fan, P. Gao, B. Liu, *Nanoscale*, 2017, **9**, 5141-51447.
- A. Lueking, R. T. Yang. *Journal of Catalysis*, 2002, **206**, 165-168.
- C. H. Chen, C. C. Huang, *Microporous and Mesoporous Materials*, 2008, **109**, 549-559.
- Kuan-Yu Lin, Wen-Ta Tsai, Tsong-Jen Yang, *Journal of Power Sources*, 2011, **196**, 3389–3394.
- S. Eugenio, U. B. Demirci, T. M. Silva, M. J. Carmezim, M. F. Montemor, *International Journal of Hydrogen Energy*, 2016, **41**, 8438-8448.
- F. Yang, Y. Zhang, P. F. Liu, Y. Cui, X. R. Ge, Q. S. Jing, *International Journal of Hydrogen Energy*, 2016, **41**, 6773-6780.
- K. Hassan, A. S. M. I. Uddin, G. S. Chung. *International Journal of Hydrogen Energy*, 2016, **41**, 10991-11001.
- K. Kim, J. I. Han, *International Journal of Hydrogen Energy*, 2015, **40**, 4567-4572.
- K. More, C. Yu, Z. Liu, S. Kaya, D. Nordlund, H. Ogasawara, *Nature Chemistry*, 2010, **2**, 454-460.
- Y. Guo, G. Lu, *International Journal of Hydrogen Energy*, 2016, **41**, 6706-6712.
- S. K. Singh, A. K. Singh, K. Aranishi, Q. Xu, *Journal of the American Chemical Society*, 2011, **133**, 19638-19641.
- S. Chen, B. D. Adams, A. Chen, *Electrochimica Acta*, 2010, **56**, 61–67.
- Y. Lu, R. Jin, W. Chen, *Nanoscale*, 2011, **3**, 2476-2480.
- H. Li, H. Y. Xu, W. Z. Li, *Journal of Membrane Science*, 2008, **324**, 44.
- K. Santhi, T. A. Revathy, V. Narayanan, A. Stephen, *Applied Surface Science*, 2014, **316**, 491-496.
- S. Liu, L. Yin, Y. Koltypin, A. Gedanken, X. Xu, Y. Yeshuru, I. Felner, G. Gorodetsky, *Journal of Magnetism and Magnetic Materials*, 2001, **233**, 195–204.
- J. M. Abdul, L. H. Chown, *International Journal of Hydrogen Energy*, 2016, **41**, 2781-2787.
- J. H. Yoo, G. Shim, S. W. Cho, C. N. Park, *International Journal of Hydrogen Energy*, 2007, **32**, 2977–2981.
- L. X. Chen, Y. F. Zhu, C. C. Yang, Z. W. Chen, D. M. Zhang, Q. Jiang, *Journal of Power Sources*, 2016, **333**, 17-23.
- D. Heon Lee, M. Kang, S. M. Paek, H. Jung, *Electrochimica Acta*, 2016, **217**, 132–138.
- T. K. Nielsen, K. Manickam, M. Hirscher, F. Besenbacher, T. R. Jensen, *ACS Nano*, 2009, **3**, 3521-3528.
- X. H. Tan, C. T. Harrower, B. S. Amirkhiz, D. Mitlin, *International Journal of Hydrogen Energy*, 2009, **34**, 7741-7748.
- H. Barlag, L. Opara, H. Zuchner, *Journal of Alloys and Compounds*, 2002, **330**, 434-437.
- Z. Zhang, Z. Zhou, S. Nie, H. Wang, H. Peng, G. Li, K. Chen, *Journal of Power Sources*, 2014, **267**, 388-393.
- Z. Hong, M. Wei, T. Lan, G. Cao, *Nano Energy*, 2012, **1**, 466-471.
- X.W. Lou, L.A. Archer, *Advanced Materials*, 2008, **20**, 1583.
- S. T. Myung, N. Takahashi, S. Komaba, C. S. Yoon, Y. K. Sun, K. Amine, H. Yashiro, *Advanced Functional Materials*, 2011, **21**, 3231-3241.
- Y. Peng, Z. Le, M. Wen, D. Zhang, Z. Chen, H. B. Wu, H. Li, Y. Lu, *Nano Energy*, 2017, **35**, 44-51.

- 46 B. Qiu, M. Xing, J. Zhang, *Journal of the American Chemical Society*, 2014, **136**, 5852–5855.
- 47 Z. Chen, Y. Yuan, H. Zhou, X. Wang, Z. Gan, F. Wang, Y. Lu, *Advanced Materials*, 2014, **26**, 339–345.
- 48 E. Liu, J. Wang, J. Li, C. Shi, C. He, X. Du, N. Zhao, *International Journal of Hydrogen Energy*, 2011, **36**, 6739–6743.
- 49 S. Rather, N. Mehraj-ud-din, R. Zacharia, S. W. Hwang, A. R. Kim, K. S. Nahm, *International Journal of Hydrogen Energy*, 2009, **34**, 961–966.
- 50 S. Liu, R. Yuan, Y. Chai, H. Su, *Sensors and Actuators*, B 2011, **156**, 388–394.
- 51 Y. Wu, J. Zhang, L. Xiao and F. Chen, *Applied Surface Science*, 2010, **256**, 4260–4268.
- 52 M. S. Dresselhaus, G. Dresselhaus, R. Saito, A. Jorio, *Physics Reports*, 2005, **409**, 47–99.
- 53 A. Reyhani, S. Z. Mortazavi, A. Z. Moshfegh, A. Nozad Golikand, M. Amiri, *Journal of Power Sources* 2009, **188**, 404–410.
- 54 M. Kaur, K. Pal, *International Journal of Hydrogen Energy*, 2016, **41**, 21861–21869.
- 55 M. Latroche, *Journal of Physics and Chemistry of Solids*, 2004, **65**, 517–522.
- 56 Ch. Chang, P. Gao, D. Bao, L. Wang, Y. Wang, Y. Chen, X. Zhou, Sh. Sun, G. Li, P. Yang, *Journal of Power Sources*, 2014, **255**, 318–324.
- 57 S. Li, W. Pan, Z. Mao, *International Journal of Hydrogen Energy*, 2005, **30**, 643–648.
- 58 X. Chen, X. P. Gao, H. Zhang, Z. Zhou, W. K. Hu, G. L. Pan, *Journal of Physical Chemistry, B* 2005, **109**, 11525–11529.
- 59 R. Akbarzadeh, M. Ghaedi, S. Nasiri Kokhdan, R. Jannesar, F. Sadeghfar, F. Sadri, L. Tayebi, *International Journal of Hydrogen Energy*, 2018, **43**, 18316–18329.
- 60 C. C. Yang, Y. J. Li, W.H. Chen, *International Journal of Hydrogen Energy*, 2010, **35**, 2336–2343.
- 61 S. C. Mu, H. L. Tang, S. H. Qian, M. Pan, R. Z. Yuan, *Carbon*, 2006, **44**, 762–767.
- 62 R. Jianwei, L. Shijun, L. Junmin, *Chinese Science Bulletin*, 2006, **51**, 2959–2963.
- 63 H. Zhang, X. Fu, J. Yin, C. Zhou, Y. Chen, M. Li, A. Wei, *Physics Letters, A* 2005, **339**, 370–377.

- Hydrogen storage capacity of (0.04)Fe-Ag/TiO₂/CNT electrode is 10.94 wt% which is nearly 5 times higher than the pristine MWCNTs.

